Current Materials Science

COUNTRY	SUBJECT AREA AND CATEGORY	PUBLISHER	H-INDEX
Netherlands Universities and research institutions in Netherlands Media Ranking in Netherlands	Materials Science └ Materials Science (miscellaneous)	Bentham Science Publishers B.V.	17

PUBLICATION TYPE	ISSN	COVERAGE	INFORMATION
Journals	26661462, 26661454	2019-2022	Homepage How to publish in this journal cms@benthamscience.net

SCOPE

Current Materials Science publishes full-length/mini reviews, research articles, recent patents and guest edited thematic issues in all areas of materials science. The journal is essential reading for all researchers involved in materials science. The journal also covers recent research in fast emerging areas of materials science, biomaterials, biological materials, magnetic materials, medical implant materials, nanomaterials, ceramics, plastics, polymers, semi-conductors, coatings, composites, paper, wood, textiles, methods, design and techniques.

Join the conversation about this journal

Current Materials Science, 2023, *16*, 352-363

RESEARCH ARTICLE

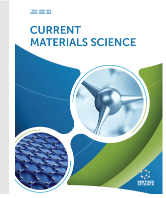

Study on the Properties of Iron-based Alloys 17-4PH Powder Manufactured by Laser Additive Manufacturing

Lei Huang[1,2], Xizhang Chen[1,2], Sergey Konovalov[1,2,3*], Chuanchu Su[1,2], Xiaoming Pan[1] and Irina Panchenko[3]

[1]Institute of Laser and Optoelectronic Intelligent Manufacturing, Wenzhou, China; [2]Samara National Research University, Samara, Russia; [3]Siberian State Industrial University, Novokuznetsk, Russia

ARTICLE HISTORY

Received: August 27, 2022
Revised: October 01, 2022
Accepted: October 24, 2022

DOI:
10.2174/2666145416666221230121951

Abstract: ***Background*:** Laser additive manufacturing has been used for surface repair and remanufacturing due to fast laser processing speed, high energy density, and dense microstructure. However, the properties of coating samples produced by laser additive manufacturing of iron-based alloys vary considerably, resulting in a large amount of data that needs to be accumulated and analyzed.

***Methods*:** The coating properties of iron-based alloy powders manufactured by laser cladding are studied. The optimal process parameters of the laser cladding are determined by exploring and comparing the macroscopic appearance, hardness, and conductivity of the junction of the cladding.

***Results*:** From the macroscopic appearance, when the ratio of the height to the width of the cladding layer is 3.615, the surface of the cladding layer has a smooth surface and is closely combined with the substrate.

***Conclusion*:** The hardness of the cladding layer is found to increase significantly, with an average hardness of 663 HV. Besides, it is found that the blackhead's hole causes the conductivity change. The ratio of the largest hole area to the smallest hole area is 8.29 times, and the depth ratio is 1.91 times, but the average resistance ratio is about 1.6 times.

Keywords: Additive manufacturing, laser cladding technology, iron-based alloy powder, hardness, conductive properties, alloys.

1. INTRODUCTION

Additive manufacturing (AM), especially the laser cladding technology, has been used for surface repair and remanufacturing due to its fast processing speed, high laser energy density, limited heat-affected zone, grain refinement of the cladding layer, dense microstructure, and conducive to automation [1-3]. Meanwhile, because of its low dilution, compact structure, and good adhesion between the coating and the base metal, this technology has been widely used in low-cost base materials, especially iron-based alloy powders like 17-4PH [4, 5]. When iron-based alloy powder is used as a processing material, laser cladding can significantly improve the base material's surface wear resistance, hardness, conductivity, and other properties [6-8]. However, with the rapid development of laser cladding and many other practical applications, the performance requirements of iron-based alloys have become more stringent, resulting in the 14-7PH stainless steel not meeting the conditions of use in some specific particular circumstances [9, 10]. Therefore, it is promising to study the properties of iron-based alloys and expand new usage scenarios.

The advanced laser cladding technology can study the parameters to prepare high-quality,

*Address correspondence to this author at the Institute of Laser and Optoelectronic Intelligent Manufacturing, Wenzhou, China; Tel: 7-3843-465883; E-mail: konovalov@sibsiu.ru

Current Materials Science

crack-free coatings. However, the layers' performances vary greatly when different laser cladding processes are chosen. Therefore, exploring the influence of specific process parameters on the coating is essential. There is much research on iron-based alloy powder's heat treatment and processing [11-18]. Mahmoudi M. *et al.* [19] investigated the mechanical properties and microstructural features of selective laser melting (SLM) using 17-4PH SS, indicating that the post-SLM heat treatment positively affected the partial strength and hardness but reduced the ductility conversely. Furthermore, as the cooling rate is relatively low, the longer interlayer time intervals between the melting of successive layers contribute to the higher austenite content, decreasing the material's hardness.

Besides, some other research focused on improving coatings' performance through thermal processing or optimized methods. These researches suggest strategies that can enhance the performance or play an essential role in predicting the performance of the layer. For example, Shi J. *et al*. [20] evaluated the effect of the sintering temperature, holding time, heating rate, and the pre-sintering stage in microwave-assisted sintering. The results have demonstrated that microwave-assisted sintering produced significantly better mechanical properties than conventional sintering in the 17-4PH stainless steel powder. Sun Y. [21] investigated conventional solutionizing and precipitation hardening (H-900) heat treatments on 17-4PH SS and wrought components; microstructural studies have shown that the 17-4PH SS components have been used to achieve microstructure and hardness similar to those of wrought samples by post-built heat treatments. Other studies focusing on the preparation process of the 17-4PH powder [22-30] have made significant progress. Kruth J. [24] studies the different appearing phenomena and process optimization. The results have shown that the process optimization, including an appropriate process parameter adjustment and the application of particular scanning strategies, the resulting parts were characterized by specific microstructure, density, and mechanical properties. However, few published studies focus on the electrical conductivity of the 17-4PH powder cladding layer.

In this work, the 17-4PH powder is processed according to the single-factor orthogonal variable method, and the macroscopic appearance and surface hardness are analyzed. Then, the reason for the resistance change is investigated, and the conductive discontinuity in the coating cross-section is investigated. Finally, the optimal process parameters of laser cladding are determined by exploring and comparing the macroscopic appearance, hardness, and conductivity of the junction of the cladding layer.

2. MATERIALS AND METHODS

2.1. Experimental Materials

In this study, a Q235 steel (mild steel) plate having a size of 50 mm × 80 mm × 6 mm was used as the base material, and its chemical composition is shown in Table **1**. It was necessary to sand the base material with sandpaper and wash it with ethanol before the laser cladding test. The powder to be laser coated is 40-90 μm 17-4PH SS powder, with a particle size of 150-300. The composition is shown in Table **1**, and the microforming and SEM morphology of the powder are shown in Fig. (**1**)

2.2. Experimental Equipment and Methods

This experiment used a 6 kW fiber laser, water cooling system, optical system, robot system, protecting gas system, and cladding head system. The working principle of the laser cladding processing system is shown in Fig. (**2**).

The 6 kW fiber laser (Rofin FL060, Rofin, Germany) (5mm × 5mm square spot) was used in the test, and the high purity argon gas (99%) was used for the tests as the carrier powder, and the protective cladding molding. It had four output light paths for laser cutting, welding, and cladding. The laser cladding system included a water-cooled system to cool the laser and the cladding head. The communication system used the (central processing unit) PLC (S7-1200, Siemens, Germany) to identify and process various signals during the test. ABB robotic motion unit is the unit that executes motion commands issued by the user. The primary function of the powder feeder is to transport the 17-4PH iron-based alloy powder uniformly and then send it to the laser cladding head composite system. The powder feeding method was coaxial argon gas feeding, and the powder feeding amount was controlled by adjusting the powder disk rotation speed and the argon

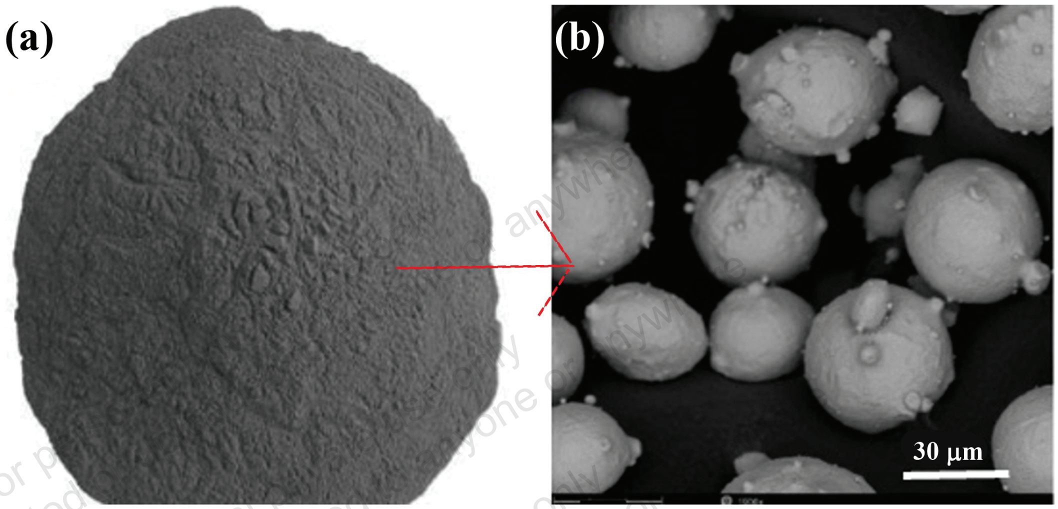

Fig. (1). The macro-forming and SEM morphology of the powder. (**a**) macro forming of 17-4PH powder. (**b**) the SEM morphology of the 17-4 power. (*A higher resolution / colour version of this figure is available in the electronic copy of the article*).

Table 1. Chemical composition table of Q235 and 17-4PH powder (wt. %).

-	C	Cr	Ni	S	P	Si	Mn	Cu	Fe
Q235	0.16	-	-	0.026	0.031	0.14	0.53	-	Remain
17-4PH	0.07	15.5	3.0	0.027	0.056	0.054	0.032	5	Remain

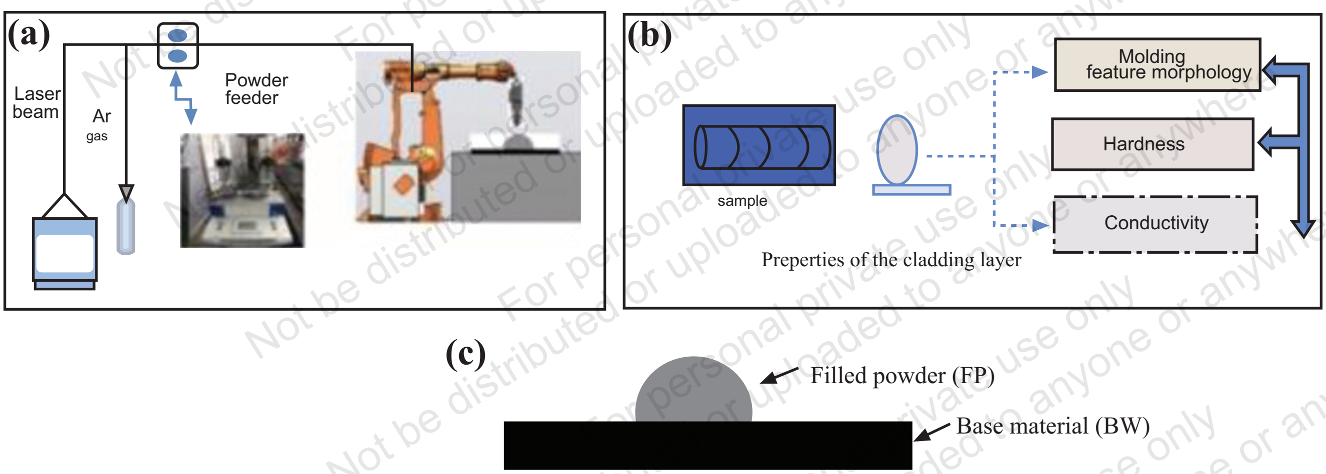

Fig. (2). The schematic layout of the laser cladding processing system (**a**) Schematic test diagram. (**b**) The research purpose of the experiment. (**c**) The schematic shape of the coating. (*A higher resolution / colour version of this figure is available in the electronic copy of the article*).

gas flow rate. The model of the feeder is a GTV PF2/2 powder feeder.

The test instruments were mainly hardness testers (HVS-50, Shanghai Yanrun Optical Machinery Technology Co., Ltd. China), wire electric discharge machines (DK7725E, Zhongyuan Lathe, China), memory oscilloscopes (SDS310 4X, RIGOL, China), and 3D laser confocal microscope (LSM 900, Carl Zeiss, Germany). The wire electric discharge machine was used to prepare the coating cross-sections. The memory oscilloscope grabbed the pulse discharge voltage and current waveform when cutting the sample to record the process parameters of the cutting section. In addition, the memory oscilloscope was used to measure changes in resistance, which was presented by current and voltage. If the resistance changes significantly, the changes in current and voltage after power-on can reflect this change instantly. Moreover, the hardness tester was used to detect the hardness of the coating and the base materials. The laser confocal microscope was used to observe the points of discontinuity in conduction and to measure the depth and area of the black spots and holes inside.

In this experiment, the single-factor orthogonal variable method was used to explore the optimal process parameters and study the effects under different laser processing parameters (laser power, scanning speed, powder feeding speed, and the carrier gas rotating speed) on the macroscopic appearance and hardness of laser cladding. Four sets are set to run the tests smoothly and obtain convincing results. Then three parameters are fixed with a variable parameter, and the cladding formation is compared. After that, it was time to measure the vertical direction of the cladding of hardness values. Five times in one cladding were estimated every 2 mm in the vertical direction of the cladding. The maximum and minimum values were removed, and the mean hardness value was finally calculated. After the laser cladding was completed, the cladding sample needed to be cut with an electric spark wire in the direction of the vertical laser scanning surface. After the cross-section was polished, it was etched with an etching solution of 96 mL H_2O: 2 mL HF: 2 mL HNO3. Laser confocal electron microscopy detected the sample sections' macroscopic appearance and breakpoint defects.

A 6 kW Rolfin laser was used to provide the heat source. Different powers, scanning speeds, powder feeding speeds, and carrier gas rotating speeds were selected to compare the coating of the laser cladding. The comparison of the hardness and macroscopic appearance determined the optimum process parameters. The single-factor testing process was established.

When the laser power was 2000 W, 2500 W, and 3000 W, respectively, the scanning speed was seven mm/s, the carrier gas rotating speed was 0.8 r/min, and the powder feeding speed was 8 mL/min. When the scanning speed was 6 mm/s, 7 mm/s, and 8 mm/s, respectively, the laser power was 2500 W, the powder feeding speed was 8 mL/min, and the carrier gas rotating speed was 0.8 r/min. When the carrier gas rotating speeds were 0.6 r/min, 0.8 r/min, and 1.0 r/min, respectively, the laser power was 2500 W, the scanning speed was 7 mm/s, and the powder feeding speed was 8mL/min. When the powder feeding speed was 7 mL/min, 8 mL/min, and 9 mL/min, respectively, the laser power was 2500 W, and the scanning speed was 7 mm/s, the carrier gas rotating speed was 0.8 r/min (the powder feeding rate was 22.4 g/min). A total of nine tests were required.

3. RESULTS AND DISCUSSION

3.1. Macroscopic Appearance Analysis

After laser cladding, it is necessary to compare those macroscopic appearances (Fig. **3**). It can be seen from the appearance that when the energy density is low, the fusion between the coating layer and the base material is insufficient. The surface smoothness of S1 is also tiny. When the laser density was increased, the unfused phenomenon was improved, and the smoothness of the cladding layer surface was also modified. When the laser power was 2500 W, the scanning speed was seven mm/s, the powder feeding speed was 8mL/min, and the carrier gas rotating speed was 0.8 r/min (Powder feeding rate 22.4 g/min), the fusion condition reached the optimum state at this time, and the width to height ratio of the surface was suitable (W2 / S2 = 4.7/1.3 = 3.615). When the energy density increases, the surface smoothness of S3 increases too much, over-increasing at the junction of the base metal and the cladding layer. In addition, the increase in the surface smoothness was more significant than the increase in the single-layer cladding width, which was not conducive to improving the surface flatness of the cladding layer [16].

The process parameters greatly influence the surface forming quality and control the energy input, which determines the processing quality. When the laser power was 2500W, the scanning speed was 7 mm/s, the powder feeding speed was 8 mL/min, and the carrier gas rotating speed was 0.8 r/min (powder feeding rate 22.4 g/min), the laser energy density at this time was conducive to surface forming. At this time, the ratio of the height to width of the cladding layer was 3.615, and the coating surface obtained was flat and tightly bonded to the base material, with no pits occurring on both sides.

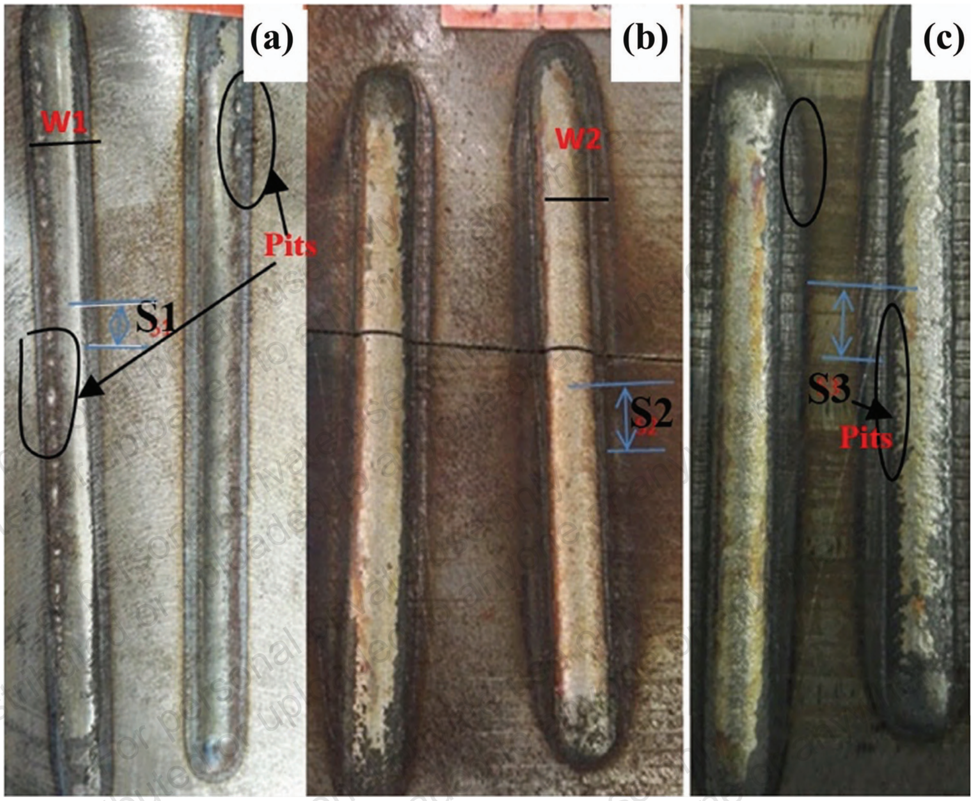

Fig. (3). Macroscopic appearance. (**a**) Power 2000 W, scanning speed 7 mm/s, powder feeding speed 8 mL/min, and carrier gas rotating speed 0.8 r/min. (**b**) Power 2500 W, scanning speed 7 mm/s, powder feeding speed 8mL/min, carrier gas rotating speed 0.8 r/min. (**c**) Power 3000W, scanning speed 7 mm/s, powder feeding speed 8 mL/min, and carrier gas rotating speed 0.8 r/min. (*A higher resolution / colour version of this figure is available in the electronic copy of the article*).

3.2. Surface Hardness Test and Analysis of Cladding Layer

After the surface polishing and finish machining of the coated samples, the hardness of the section and surface of the cladding of the six selected model points were measured with a Rockwell hardness tester. The highest and lowest values were removed to reduce the impact on the hardness data, and the mean value of the rest was calculated. The results showed that the average hardness of the coating was 663 HV, and the average hardness of the base material was 358 HV, which was about 1.85 times higher than that of the base material. The results are shown in Fig. (**4**).

The process parameters have an essential influence on surface hardness. With the increase of laser power (2000-3000w), the ratio of the height to width of the cladding layer gradually increased, and the hardness at this time increased first and then decreased. Finally, when the laser power was 2500w, the hardness reached the maximum value. Also, with the increasing scanning speed (6-8mm/s), the ratio of the height to width of the cladding layer gradually decreased, and the hardness increased first and then decreased. When the scanning speed was 7mm/s, the hardness reached the maximum value. And the powder feeding speed and the carrier gas rotating speed also had such changes, as shown in Fig. (**4**).

Therefore, appropriate process parameters can obtain better surface hardness of the coating. Comparing the hardness of the base material and the cladding layer, it was found that when the cladding power was 2500 W, the scanning speed was 7 mm/s, the powder feeding speed was 8 mL/min, and the carrier gas rotating speed was 0.8 r/min (powder feeding rate 22.4 g/min), the surface hardness is the best at this time. The results indicated that the average hardness of the coating was 663 HV, and the highest hardness of the cladding layer was 736 HV.

3.3. Microscopic Observation and Conductivity Analysis

The electric spark cutting was used in the test, and it was found that when the cutting was close to the breaking point, it was challenging to continue the cutting, so the operation was stopped. When cutting the cladding layer with the electric spark, it was found that most of the cuts were stopped in the middle of the cladding layer. After cutting, one cladding layer can continue to be cut in the middle of the coating, and the process parameter laser power was 2500 W, the scanning speed was 7 mm/s, the powder feeding speed was 8 mL/min, the carrier gas rotating speed was 0.8 r/min (powder feeding rate 22.4 g/min). Therefore, it would be concluded that the resistance was the smallest at this time. Besides, the macroscopic morphology of multipass laser cladding coating is shown in Fig. (**5**). The process parameters of electric spark cutting are shown in Table **2**. The memory oscilloscope captures the single-pulse discharge voltage and current waveforms, as shown in Fig. (**6**). Due to the characteristics of the high-frequency power source, the sustained voltage of the discharge remained substantially unchanged during the discharge process. Still, the current changed as the discharge continued. It can be indicated that the laser cladding was coated under the influence of the high temperature and heat conduction of the discharge channel.

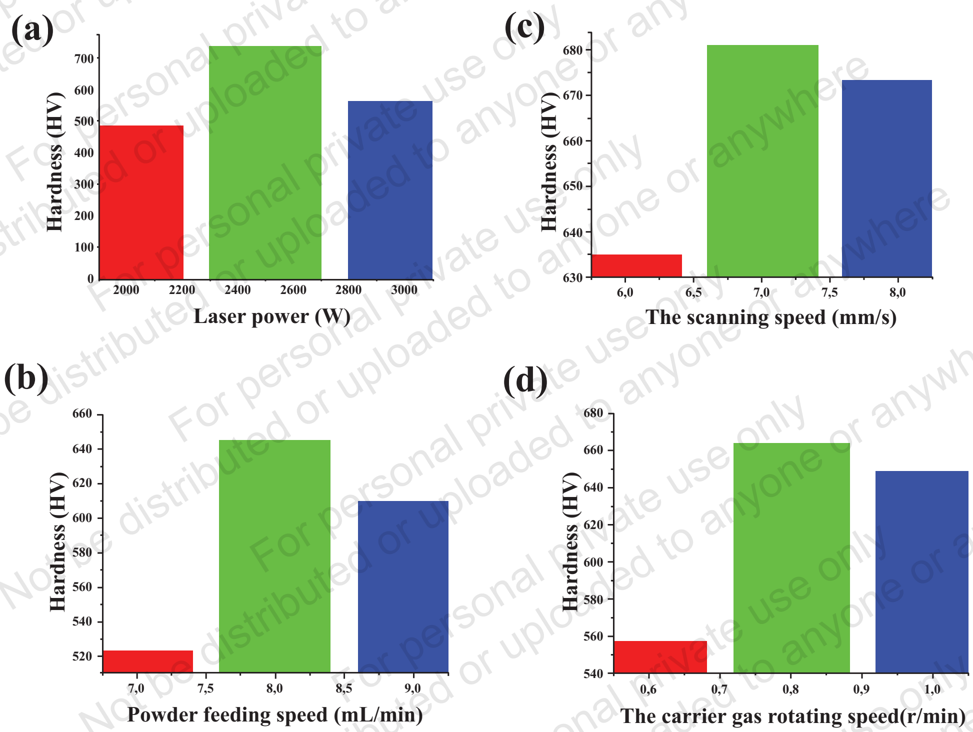

Fig. (4). Effect of laser cladding process parameters on joint hardness. (**a**) The effect of laser power on hardness. (**b**) The effect of scanning speed on hardness. (**c**) The effect of powder feeding speed on hardness.(**d**) The effect of the carrier gas rotating speed on the hardness. (*A higher resolution / colour version of this figure is available in the electronic copy of the article*).

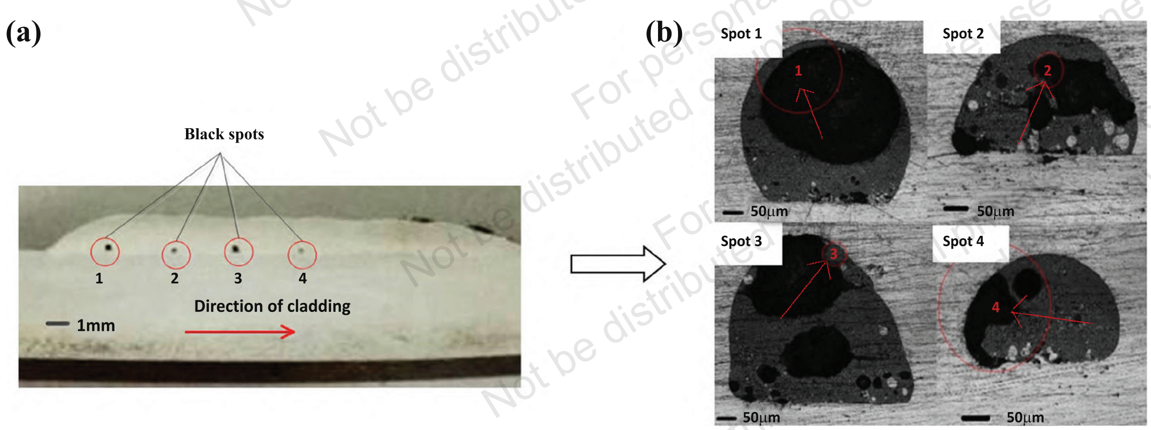

Fig. (5). Macroscopic morphology of laser cladding coating (**a**) The appearance size of the coating; (**b**) 2D topography of black spot1-4. (*A higher resolution / colour version of this figure is available in the electronic copy of the article*).

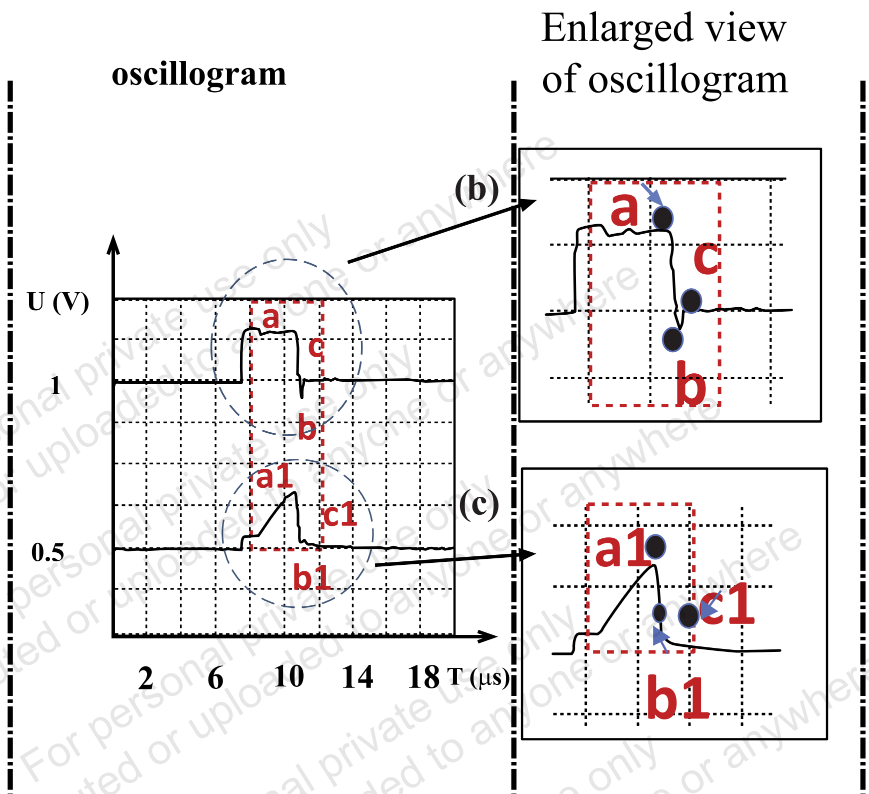

Fig. (6). Single pulse voltage and current oscillogram. (**b**) Enlarged view of the oscillogram of 1.0 V voltage. (**c**) Enlarged view of the oscillogram of 0.5 V. (*A higher resolution / colour version of this figure is available in the electronic copy of the article*).

Table 2. Process parameters of WED.

Process Parameter	Value
Way of entering	Positive processing
Discharge voltage	160 V
Pulse width	32 μm
Duty cycle	1:8
Feed rate	20 μm
Wire-speed	10 m/s
Average machining current	2.5A

The oscillogram is the resistance test at the hole shown in Fig. (**6**). From a to b to c, and from a1 to b1 to c1 is the resistance test at the hole (a represents the maximum voltage at the hole, b represents the minimum voltage at the hole, and c represents the voltage at the non-hole. Similarly, a1 represents the maximum voltage at the hole, b represents the minimum voltage at the hole and c1 at the non-hole). It can be seen from the red thick line box in the single pulse discharge voltage and current waveform, from point a1 to point b1, the voltage and current of the laser cladding are sharply decreasing while the external supply voltage was 160 V, which was unchanged. According to R=U/I, the electrical resistance increases sharply at this time; from point b to point c, the voltage is reversed. The external circuit is not turned on, and an internal reverse-induced voltage is formed simultaneously. Simultaneously, the resistance ratio of a,b, and c can be obtained, of which Rb/Ra was 1.6.

The energizing of the cladding layer is analyzed, and the following electrical model is established, as shown in Fig. (**7**). Fig. (**7b**) simplified the induced current to ease the calculation. Through the analysis, Rb/Ra=1.6, and the calculation method is shown in equations (1 and 2):

$$\begin{cases} R_a I_1 = 1.15 \\ R_b I_2 = 0.95 \\ R_a I_3 = 0.525 \\ R_b I_4 = 0.675 \\ R = \dfrac{\triangle U}{\triangle I} \end{cases} \tag{1}$$

$$\frac{R_b}{R_a} = 1.6 \tag{2}$$

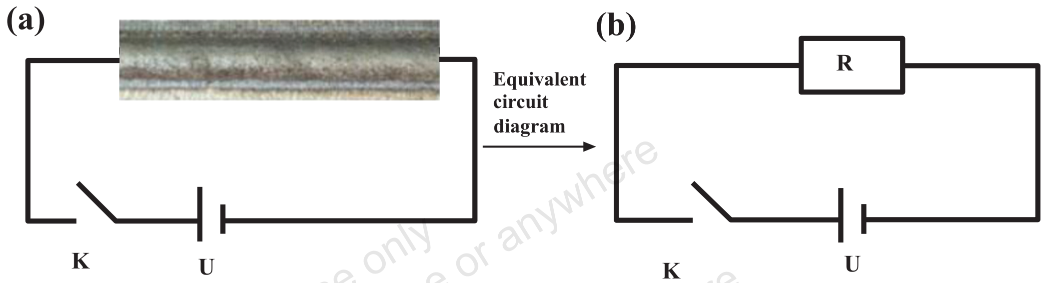

Fig.(7). Induction circuit (**a**) Inductive electrical model of coating, (**b**) Simplified model of inductive electrical.

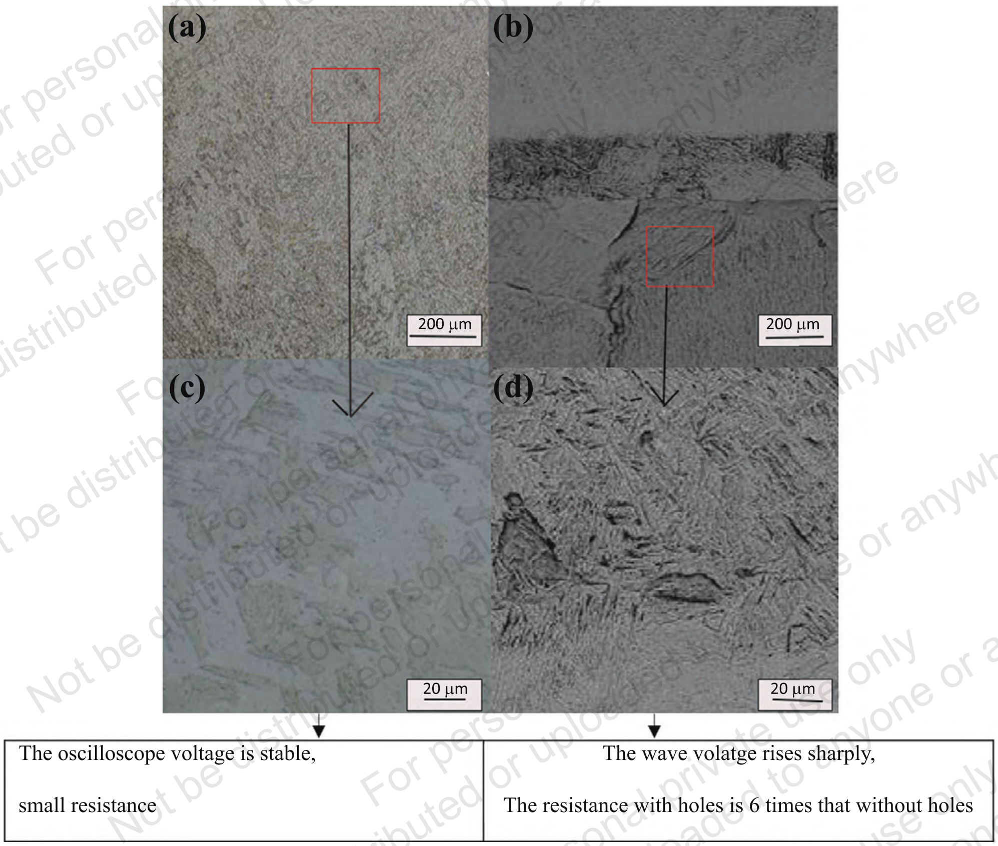

Fig.(8). (**a** and **c**) Microscopic morphology of areas without black spots. (**b** and **d**) The microscopic morphology of the site is close to the black holes. (*A higher resolution / colour version of this figure is available in the electronic copy of the article*).

After that, a laser confocal microscope was used to observe the vicinity of the cross-section's breakpoint, obtaining the microscopic 2D morphology and the local 3D cloud topography of the black spots near and without the black spots.

Fig. (**8**) shows that the microstructure of the coating with no change in the resistive layer is uniform. However, there are also pores near the breakpoint in the microstructure of the coating where the resistance changes. Furthermore, through the detection of the microstructure of several other sets, it is found that there are pores in the microstructure of the coating. Pores affect the roughness and the area where the pores exist, and the electrical conductivity is generally poor. Besides, as the laser power density increases, the ratio of the surface of the deposited layer gradually increases. At the same time, the equiaxed crystal and cellular crystal structure near the center first increase and then decrease. The dendritic crystal and plate crystal structure increase, causing the hardness decreases after the rise.

The three-dimensional structure of the coating varies greatly, which is closely related to the change in resistance. Fig. (**8**) indicates that the uniform structure has a small impact on resistance, but the pores of the microstructure have a large impact on resistance. However, at the

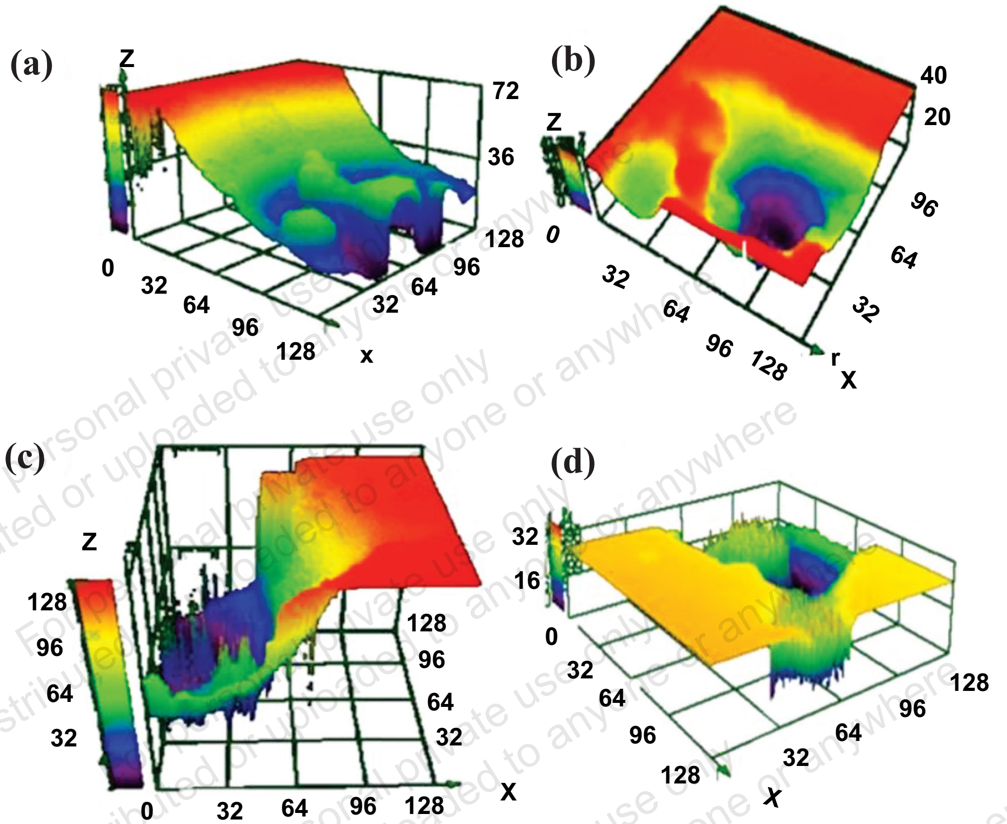

Fig. (9). 3D cloud topography of black spots 1-4. (**a**) Spot 1. (**b**) Spot 2. (**c**) Spot 3. (**d**) Spot 4. (*A higher resolution / colour version of this figure is available in the electronic copy of the article*).

Table 3. Geometric parameters of black points.

No.	Area of Black Spot, μM2	Hole Area, (MM2)	Maximum Hole Depth, (MM)
spot 1	105635.17	58064.26	78.61
spot 2	47495.99	15598.90	46.21
spot 3	116806.41	40268.38	134.13
spot 4	29319.40	6798.43	41.22

three-dimensional level of the coating, the microstructure changes considerably, the inhomogeneity of the structure increases, and the influence of the three-dimensional structure on the resistance is unclear. As a result, it is necessary to test coatings with low microstructure to explore the impact of electrical conductivity and the microstructure of the coating.

Fig. (**9**) shows the vicinity of the 3D cloud topography and the area of each black spot. It can be observed from the 3D cloud topography that the black spots were concave holes that collapsed inward. When the current passes through the concave hole, the electrical resistance in the circuit sharply increases, causing the cut of the current and disconnecting the circuit. The depth of each black spot measured by the laser confocal microscope is shown in Table **3**.

From the two-dimensional topography, it can be seen that black spots have appeared near the point where the current cut. With the help of the laser confocal microscope, the geometric parameters of the black spots and the concave holes are shown in Table **3**. The data in Table **3** indicates that the area of the black dots and the maximum hole depth alternate according to size.

By testing the influence of the electric discharge wire cutting near the black spots on the cross-section of the multipass laser cladding coating, it was found that the whole area and the hole depth had a particular influence on the black point conductivity. The larger the hole area and the deeper the hole, the worse the conductivity. By analyzing the microstructure, it was found that the hole caused the conductivity change. The ratio of the largest hole area to the smallest hole area is 8.29 times, the depth ratio is 1.91 times, and the mean resistance ratio is 1.6 times.

The noticeable increase in resistance at the cladding junction is the presence of the groove depth. The sharp increase in the electrical resistance of black spots is due to the rise of the groove depth and the hole area. The holes act as a vital electrical resistance or switch in this circuit, causing the current to be discontinuous or blocked.

CONCLUSION

In this study, the optimal process parameters are obtained by studying the junction's microscopic appearance, hardness, and electrical conductivity between the cladding layer. The following conclusions can be drawn.

(1) When the ratio of the height to width of the coating layer is 3.615, the coating layer has a smooth surface, combined with the base material closely, and has no pits on both sides.

(2) Compared with the hardness of the base metal and the cladding layer, the hardness of the cladding layer is significantly improved, 1.85 times higher than that of the base metal.

(3) The microstructure influences the conductivity. The larger the hole on the coating surface and the deeper the hole, the worse the conductivity of the coating. The microstructure influences the conductivity; the larger the pores on the coating surface and the deeper the pores, the worse the conductivity of the coating. By analyzing the microstructure, it was found that the hole caused the conductivity change. The ratio of the largest hole area to the smallest hole area is 8.29 times, and the depth ratio is 1.91 times, but the average resistance ratio is about 1.6 times.

(4) The optimum process parameters for single laser cladding: laser power was 2500 W, scanning speed was 7 mm/s, powder feeding speed was 8 mL/min, and the carrier gas rotating speed was 0.8 r/min (powder feeding rate 22.4 g/min). At this time, it has maximum hardness and an excellent macro appearance.

CONSENT FOR PUBLICATION

Not applicable

AVAILABILITY OF DATA AND MATERIALS

The data supporting this study's findings are available within the article.

FUNDING

This work was sponsored by the National Natural Science Foundation of China under Grants No. 51975419 and 51575401, Wenzhou major scientific and technological innovation project under Grant No. ZG2020029 and within the framework of the state task of the Ministry of Science and Higher Education of the Russian Federation No. 0809-2021-0013.

CONFLICT OF INTEREST

The authors declare no conflict of interest.

ACKNOWLEDGEMENTS

We are grateful to Wenzhou University and the China Scholarship Committee for providing research grants to Samara National Research University and Siberian State Industrial University to improve experiments.

REFERENCES

[1] Zhu L, Xue P, Lan Q, *et al*. Recent research and development status of laser cladding: A review. Opt Laser Technol 2021; 138: 106915. http://dx.doi.org/10.1016/j.optlastec.2021.106915

[2] Liu Y, Li C, Huang XF, Zhang HY, Li C. Investigation on solidification structure and temperature field with novel processing of synchronous powder-feeding underwater laser cladding. J Mater Process Technol 2021; 296: 117166. http://dx.doi.org/10.1016/j.jmatprotec.2021.117166

[3] Geng Y, Konovalov SV, Chen X. Research status and application of the high-entropy and traditional alloys fabricated *via* the laser cladding. Uspehi Fiziki Metallov 2020; 21(1): 26-45.

http://dx.doi.org/10.15407/ufm.21.01.026

[4] Nie MH, Zhang S, Wang ZY, Zhang CH, Chen HT, Chen J. Effect of laser power on microstructure and interfacial bonding strength of laser cladding 17-4PH stainless steel coatings. Mater Chem Phys 2022; 275(1): 125236. http://dx.doi.org/10.1016/j.matchemphys.2021.125236

[5] Wang Y, Chen X, Konovalov SV. Additive manufacturing based on welding arc: a low-cost method. J Surf Invest X-ray, Synchrotron Neutron Tech 2017; 11(6): 1317-28. http://dx.doi.org/10.1134/S1027451017060210

[6] Lei J, Shi C, Zhou S, Gu Z, Zhang LC. Enhanced corrosion and wear resistance properties of carbon fiber reinforced Ni-based composite coating by laser cladding. Surf Coat Tech 2018; 334: 274-85. http://dx.doi.org/10.1016/j.surfcoat.2017.11.051

[7] Chen D, Konovalov S, Golubeva A, *et al*. Microstructural characterization of coatings produced by selective laser melting of ni-powder on titanium alloy substrate. Int J Robot Res 2020; 9(7): 954-9. http://dx.doi.org/10.18178/ijmerr.9.7.954-959

[8] Chiboub Fellah FZ, Pointillart F, Guizouarn T, *et al*. Photophysical properties and single - molecule magnet behavior in heterobimetallic 3d4 f schiff base complexes. Eur J Inorg Chem 2022; 2022(27): 27.1-8.doi.org/10.1002/ejic.202200349 http://dx.doi.org/10.1002/ejic.202200349

[9] Park DY, Lee GM, Kwon YS, *et al*. Investigation of powder size effects on sintering of powder injection moulded 17-4PH stainless steel. Powder Metall 2017; 60(2): 139-48. http://dx.doi.org/10.1080/00325899.2017.1278911

[10] Meredith SD, Zuback JS, Keist JS, Palmer TA. Impact of composition on the heat treatment response of additively manufactured 17–4 PH grade stainless steel. Mater Sci Eng A 2018; 738: 44-56. http://dx.doi.org/10.1016/j.msea.2018.09.066

[11] Chen X, Huang Y, Madigan B, Zhou J. An overview of the welding technologies of CLAM steels for fusion application. Fusion Eng Des 2012; 87(9): 1639-46. http://dx.doi.org/10.1016/j.fusengdes.2012.06.009

[12] Masoomi M, Shamsaei N, Winholtz RA, *et al*. Residual stress measurements *via* neutron diffraction of additive manufactured stainless steel 17-4 PH. Data Brief 2017; 13: 408-14. http://dx.doi.org/10.1016/j.dib.2017.06.027 PMID: 28664178

[13] Yao J, Wang L, Zhang Q, Kong F, Lou C, Chen Z. Surface laser alloying of 17-4PH stainless steel steam turbine blades. Opt Laser Technol 2008; 40(6): 838-43. http://dx.doi.org/10.1016/j.optlastec.2007.11.008

[14] Pasebani S, Ghayoor M, Badwe S, Irrinki H, Atre SV. Effects of atomizing media and post processing on mechanical properties of 17-4 PH stainless steel manufactured *via* selective laser melting. Addit Manuf 2018; 22: 127-37. http://dx.doi.org/10.1016/j.addma.2018.05.011

[15] Kudzal A, McWilliams B, Hofmeister C, *et al*. Effect of scan pattern on the microstructure and mechanical properties of powder bed fusion additive manufactured 17-4 stainless steel. Mater Des 2017; 133: 205-15. http://dx.doi.org/10.1016/j.matdes.2017.07.047

[16] Supriadi S, Dewantoro S, Mawardi FA, Irawan B, Doloksaribu M, Suharno B. Preparation of feedstock using beeswax binder and SS 17-4PH powder for fabrication process of orthodontic bracket by metal injection molding. AIP Conf Proc 2019; 209(2): 020029. http://dx.doi.org/10.1063/1.5096697

[17] Demir S, Sarioğlu AO, Güler S, Dege N, Sönmez M. Synthesis, crystal structure analysis, spectral IR, NMR UV–Vis investigations, NBO and NLO of 2-benzoyl-N-(4-chlorophenyl)-3-oxo-3-phenylpropanamide with use of X-ray diffractions studies along with DFT calculations. J Mol Struct 2016; 1118: 316-24. http://dx.doi.org/10.1016/j.molstruc.2016.04.042

[18] Nevskii S, Sarychev V, Konovalov S, Granovskii A, Gromov V. Wave instability on the interface coating/substrate material under heterogeneous plasma flows. J Mater Res Technol 2020; 9(1): 539-50. http://dx.doi.org/10.1016/j.jmrt.2019.10.083

[19] Xu S, Chen X, Konovalov S. Effect of phase transition temperature and particle size on residual stresses and properties of laser cladding layer. IOP Conf Seri: Mater Sci Eng 2018; 411(1): 012084. http://dx.doi.org/10.1088/1757-899X/411/1/012084

[20] Shi J, Cheng Z, Gelin J, Barriere T, Liu B. Sintering of 17-4PH stainless steel powder assisted by microwave and the gradient of mechanical properties in the sintered body. The I J Adv Manuf Techn 2017; 91: 2895-906. http://dx.doi.org/10.1007/s00170-016-9960-y

[21] Sun Y, Hebert RJ, Aindow M. Effect of heat treatments on microstructural evolution of additively manufactured and wrought 17-4PH stainless steel. Mater Des 2018; 156: 429-40. http://dx.doi.org/10.1016/j.matdes.2018.07.015

[22] LeBrun T, Nakamoto T, Horikawa K, Kobayashi H. Effect of retained austenite on subsequent thermal processing and resultant mechanical properties of selective laser melted 17–4 PH stainless steel. Mater Des 2015; 81: 44-53. http://dx.doi.org/10.1016/j.matdes.2015.05.026

[23] Basu D, Wu Z, Meyer JLL, Larson E, Kuo R, Rollett A. Entrapped gas and process parameter-induced porosity formation in additively manufactured 17-4 PH stainless steel. J Mater Eng Perform 2021; 30(7): 5195-202. http://dx.doi.org/10.1007/s11665-021-05695-3

[24] Kruth JP, Froyen L, Van Vaerenbergh J, Mercelis P, Rombouts M, Lauwers B. Selective laser melting of iron-based powder. J Mater Process Technol 2004; 149(1-3): 616-22. http://dx.doi.org/10.1016/j.jmatprotec.2003.11.051

[25] Bermingham MJ, Kent D, Dargusch MS. A new understanding of the wear processes during laser assisted milling 17-4 precipitation hardened stainless steel. Wear 2015; 328-329(30): 518-30. http://dx.doi.org/10.1016/j.wear.2015.03.025

[26] Çetinkaya C, Fındık T, Özbilen S. Characterisation of mechanically milled 17-4 PH gas atomized stainless steel powders. Mater Des 2007; 28(1): 266-71. http://dx.doi.org/10.1016/j.matdes.2005.07.012

[27] Mazari SA, Ali E, Abro R, *et al*. Nanomaterials: Applications, waste-handling, environmental toxicities, and future challenges – A review. J Environ Chem Eng 2021; 9(2): 105028. http://dx.doi.org/10.1016/j.jece.2021.105028

[28] Yin L, Wang J, Chen X, *et al*. Microstructures and their distribution within HAZ of X80 pipeline steel welded using hybrid laser-MIG welding. Weld World 2018; 62(4): 721-7. http://dx.doi.org/10.1007/s40194-018-0582-x

[29] Gao C, Chen X, Su C, Chen X. Location dependence of microstructure and mechanical properties on wire arc additively manufactured nuclear grade steel. Vacuum 2019; 168: 108818.
http://dx.doi.org/10.1016/j.vacuum.2019.108818

[30] Osintsev KA, Konovalov SV, Gromov VE, Ivanov YF, Panchenko IA. Microstructure and mechanical properties of non-equiatomic Co25.4Cr15Fe37.9Mn3.5Ni16.8Si1.4 high-entropy alloy produced by wire-arc additive manufacturing. Mater Lett 2022; 312: 131675.
http://dx.doi.org/10.1016/j.matlet.2022.131675